Modified *GW* method in electronic systems

Zhipeng Sun [1,2] Zhenhao Fan,[1,2] Hui Li,[1,2] Dingping Li [1,2,*] and Baruch Rosenstein[3,†]

[1]*School of Physics, Peking University, Beijing 100871, China*
[2]*Collaborative Innovation Center of Quantum Matter, Beijing 100871, China*
[3]*Electrophysics Department, National Yang Ming Chiao Tung University, Hsinchu 30050, Taiwan, Republic of China*

A modified *GW* approximation to many-body systems is developed. The approximation has the same computational complexity as the traditional *GW* approach, but uses a different truncation scheme. This scheme neglects the high-order connected correlation functions. A covariant (preserving the Ward identities due to the charge conservation) scheme for the two-body correlators is employed, which holds the relation between the charge correlator and the charge susceptibility. The method is tested on the two-dimensional one-band Hubbard model. The results are compared with exact diagonalization, the *GW* approximation, the fluctuation-exchange (FLEX) theory, and determinantal Monte Carlo approach. The comparison for the (one-body) Green's function demonstrates that it is more precise in the strong-coupling regime (especially away from half filling) than the *GW* and FLEX approximations, which have a similar complexity. More importantly, this method indicates a Mott-Hubbard gap as the Hubbard *U* increases, whereas the *GW* and FLEX methods fail. In addition, the charge correlator obtained from the covariant scheme not only holds the consistency of the static charge susceptibility, but also makes a significant improvement over the random phase approximation calculations.

I. INTRODUCTION

Understanding the physics of strongly correlated electronic systems has been a challenge in condensed matter theory for many decades. These systems are hosts of distinct phenomena such as the Mott insulator [1], quantum magnetism [2], pseudogap [3], strange metals [4], and *d*-wave high-temperature superconductivity [5,6], all of which cannot be explained within the framework of the traditional renormalized weak coupling expansion. Above the atomic level (described by the density-functional approximation), the main features of these systems are typically captured sufficiently well by the lattice effective Hamiltonian with (quasi)local Coulomb repulsion. Up to now, numerous nonperturbative numerical and analytic approaches have been developed to tackle these seemingly simple models, such as the (one or multiband) Hubbard model [7].

Numerical nonperturbative methods include the density matrix renormalization group (DMRG) [8], determinantal quantum Monte Carlo (MC) simulation [9], and dynamic mean-field theory (DMFT) [10,11]. They can produce reliable results in certain cases, but have limitations in the cases of interest, for example, at very low temperature or deviations from half filling (doping). DMRG is reliable mostly in the one-dimensional case, while the determinantal MC encounters a severe fermionic sign problem and thus fails at low temperature and significant doping. DMFT, although successful at intermediate coupling, generally misses nonlocal fluctuations.

A lot of effort was made to remedy this by the extensions of a more elaborate scheme [12,13].

Analytic nonperturbative methods evolved from simple mean-field methods [2] like variations of Hartree-Fock (HF), to more sophisticated field theoretical methods. Generally, a closed set of (quite complicated) equations of the correlators and the vertex functions is constructed and subsequently solved numerically. The most used approximations are based on the Baym-Kadanoff formalism [14,15], Hedin's equations [16], and diagrammatic analysis [17]. Others are based on particular truncations of Dyson-Schwinger equations [18–20].

By their complexity, analytic methods can be broadly classified into two classes. In the simpler class, one identifies a function (or functions) of just *one* energy-momentum variable as the relevant degree of freedom. Examples include the electronic Green's function $G(\omega, k)$, the screened dynamical potential $W(\omega, k)$, and the charge and spin susceptibilities $\chi(\omega, k)$. Beyond the HF, two popular approximations of this class are the *GW* approximation [16,21], involving G and W, and the fluctuation-exchange (FLEX) theory [22], involving G and χ's. More complicated schemes such as the parquet approximation [23,24] and covariant quartic approximation [25], in addition to one-momentum functions, unfortunately have to consider *multiple*-momenta-dependent quantities, such as two-body vertex functions and high-order correlators.

To describe realistic correlated materials, complicated schemes are often not feasible yet due to their large computational complexity, and thus the simpler class is more favored. However, the current *GW* and FLEX approximation produce less accurate data compared with experimental [26] or numerically exact results [24]. Therefore, a simpler yet sufficiently reliable and precise method is highly sought after.

*lidp@pku.edu.cn
†vortexbar@yahoo.com

In this paper, one such method, a modification of *GW* approximation, is developed. To fully take advantage of the clustering properties of the connected correlators, the modified *GW* approximation is to truncating high-order connected correlators on Dyson-Schwinger equations. The resulting equations turn out be quite similar to the *GW* equations, and the physical meanings are also analogous. As in *GW*, the Coulomb interaction is renormalized and the screening for long-range interaction is included within the modified *GW* approximation. In this degree, this method is applicable to realistic materials.

In a many-body system, the charge conservation leads to a set of Ward identities. In an approximation (such as *GW* or FLEX), the Ward identity for a one-body Green's function is obeyed, whereas the Ward identity for the two-body correlator (directly obtained from equations after the approximation) is often violated. In addition, the relation between the charge correlator and charge susceptibility, $\partial n / \partial \mu = \chi^{\mathrm{ch}}(\omega = 0, k = 0)$, is often violated [27]. To preserve these identities, the covariant scheme [28–30] is employed in this paper.

The modified *GW* approximation is tested on the two-dimensional (2D) one-band Hubbard model in this paper. The results for the density and the Green's function demonstrate that the modified *GW* approximation produce satisfactory results *even in the strong-coupling regime* compared with exact diagonalization (ED) or the determinantal MC approach. The method also indicates a Mott-Hubbard gap as the Hubbard *U* increases, whereas the *GW* and FLEX methods fail. The results of the charge correlator demonstrate a significant improvement over the random phase approximation (RPA) scheme, and the charge susceptibility obtained from the covariant scheme is consistent with an independent calculation $\partial n / \partial \mu$.

This paper is organized as follows. In Sec. II, the modified *GW* approximation is presented for the fermionic (one-body) Green's function. Next, in Sec. III, the covariant scheme for the two-body correlators is presented. In Sec. IV, this method is tested on the 2D Hubbard model by comparing the (one-body) Green's function (and the density), and the (two-body) charge correlator (and the static charge susceptibility) with other approaches. The conclusions and discussions are given in Sec. V.

II. MODIFIED *GW* APPROXIMATION FOR FERMIONIC GREEN'S FUNCTION

In this section, basic equations and assumptions of the modified *GW* approximation are presented. The general density-density-type interacting fermionic system at finite temperature is considered. Two exact equations involving the connected correlators are derived. The approximation is motivated by the clustering properties of the connected correlators.

A. Two exact equations for correlators

The Matsubara action for a density-density-type interacting fermionic system at finite temperature has the form

$$S[\psi, \psi^*] = -\int d(12)\, T(1, 2)\psi^*(1)\psi(2)$$
$$+ \frac{1}{2}\int d(12)\, V(1, 2)\rho(1)\rho(2), \quad (1)$$

where ψ^*, ψ are Grassmannian fields and $\rho(1) \equiv \psi^*(1)\psi(1)$ is the density (composite operator). The label $(1) \equiv (\sigma_1, x_1, \tau_1)$ represents a generalized coordinate, containing the spin projection σ_1, the space coordinate x_1, and the Matsubara time $0 < \tau_1 < \beta$, with β being the inverse temperature. The condensed notation $\int d(1)$ stands for the integral or summation over all the values of a generalized coordinate (σ_1, x_1, τ_1). The bilocal functions T and V are the hopping strength and the interaction (dynamical) potential. Generalization to several fermionic species or type of interactions (spin, current) is straightforward.

Consider the perturbation of the system by an external bosonic source $\phi(1)$ (local spin selective chemical potential) coupled to the density:

$$S[\psi, \psi^*; \phi] = S[\psi, \psi^*] - \int d(1)\, \phi(1)\rho(1). \quad (2)$$

Note that unlike in Ref. [25], the source is coupled to a quantity quadratic in the fermionic fields. Using the grand partition function,

$$Z[\phi] = \int \mathcal{D}[\psi, \psi^*]\, e^{-S[\psi, \psi^*; \phi]}, \quad (3)$$

the (one-body) Green's function G is given by

$$G(1, 2) \equiv \langle \psi^*(2)\psi(1) \rangle$$
$$= \frac{1}{Z[\phi]} \int \mathcal{D}[\psi, \psi^*]\, \psi^*(2)\psi(1)e^{-S[\psi, \psi^*; \phi]}. \quad (4)$$

Here $\int \mathcal{D}[\psi, \psi^*]$ is the (Grassmannian) functional path integral measure.

The Green's function $G(1, 2)$ and its functional derivative $\delta G(1, 2)/\delta \phi(3)$ are related through the following equation of motion (see Appendix A1 for derivation):

$$\delta(1, 2) = \int d(3)\, H^{-1}(1, 3)G(3, 2)$$
$$- \int d(3)\, V(1, 3)\frac{\delta G(1, 2)}{\delta \phi(3)}. \quad (5)$$

Here $\delta(1, 2)$ is the Dirac/Kronecker delta function and the Hartree propagator H is defined by

$$H^{-1}(1, 2) \equiv T(1, 2) + \delta(1, 2)v(1). \quad (6)$$

Here the density weighted interaction potential v is

$$v(1) \equiv \phi(1) - \int d(2)\, V(1, 2)\rho(2). \quad (7)$$

Note that in the absence of the external source, i.e., $\phi = 0$, the quantity H is the free Green's function with Hartree self-energy absorbed in the chemical potential.

Functional derivative of Eq. (5) with respect to the source ϕ yields

$$
\begin{aligned}
0 = &\int d(4) \frac{\delta H^{-1}(1,4)}{\delta \phi(3)} G(4,2) \\
&+ \int d(4) H^{-1}(1,4) \frac{\delta G(4,2)}{\delta \phi(3)} \\
&- \int d(4) V(1,4) \frac{\delta^2 G(1,2)}{\delta \phi(3) \delta \phi(4)},
\end{aligned}
\tag{8}
$$

relating the one-body correlator G and the two-body correlator correlator $\delta G/\delta \phi$ to the three-body correlator $\delta^2 G/\delta \phi^2$. By successive functional derivatives, one can obtain a hierarchy of such relations for even higher order correlators. These are used in the search of successful nonperturbative approximations by truncating certain terms considered small by a certain qualitative argument valid for a particular class of systems and values of parameters. This way, a closed set of equations is obtained and solved numerically, typically by iterations.

B. Clustering property of connected correlators and the *HGW* truncation

The simplest approximation is to truncating $\delta G/\delta \phi$ in the first equation of motion Eq. (5). This yields $G = H$, namely, the Hartree approximation widely used in condensed-matter physics [2]. A more complicated (and hopefully precise, see below) approximation would be truncating the $\delta^2 G/\delta \phi^2$ term in Eq. (8). Justification for such a truncation originates from the clustering property, which states that the connected correlation function is very small as its coordinates are separated. The quantity

$$
\frac{\delta^2 G(1,2)}{\delta \phi(3) \delta \phi(4)} = \langle \psi^*(2) \psi(1) \rho(3) \rho(4) \rangle_{\mathrm{c}}
\tag{9}
$$

is a connected correlation function, and thus can be omitted in certain cases. The reliability of this truncation is determined by the inequality

$$
\left| \int d(45) H(1,5) V(5,4) \frac{\delta^2 G(1,2)}{\delta \phi(3) \delta \phi(4)} \right|
$$
$$
\ll \left| \int d(45) H(1,4) \frac{\delta H^{-1}(4,5)}{\delta \phi(3)} G(5,2) \right|.
\tag{10}
$$

Then one can approximate Eq. (8) by

$$
\frac{\delta G(1,2)}{\delta \phi(3)} = - \int d(45) H(1,4) \frac{\delta H^{-1}(4,5)}{\delta \phi(3)} G(5,2).
\tag{11}
$$

The validity of inequality Eq. (10) will be indirectly checked by whether the Green's function obtained within the approximation is in good agreement with the numerically exact results.

Equations (5) and (11) form a closed set and will yield the *HGW* equations (for derivation, see Appendix B1):

$$
G^{-1}(1,2) = H^{-1}(1,2) - \Sigma(1,2),
\tag{12a}
$$

$$
\Sigma(1,2) = -H(1,2) W(2,1),
\tag{12b}
$$

$$
W^{-1}(1,2) = V^{-1}(1,2) - \Pi(1,2),
\tag{12c}
$$

$$
\Pi(1,2) = H(1,2) G(2,1).
\tag{12d}
$$

TABLE I. Comparison between the *HGW* and *GW* equations.

	HGW	*GW*
Equation for G	$G^{-1} = H^{-1} - \Sigma$	
Equation for Σ	$\Sigma = -HW$	$\Sigma = -GW$
Equation for W	$W^{-1} = V^{-1} - \Pi$	
Equation for Π	$\Pi = HG$	$\Pi = GG$
Approximation	$\delta^2 G/\delta \phi^2 = 0$	$\Lambda = \hat{1}$

Apparently, these equations resemble those of the *GW* approximation (see Ref. [21] or Appendix F). The equations Eq. (12a) for Green's function G and Eq. (12c) for screened dynamical potential W are the same, whereas the equations Eq. (12b) for self-energy function Σ and Eq. (12d) for polarization function Π are different. The *HGW* approximation is named due to its the similarity to the *GW* approximation and Hartree approximation. Some of the propagators G in *GW* equations are replaced by the Hartree propagator H in the *HGW* equations.

Essentially, the *HGW* equations and *GW* equations are based on different approximation schemes. The *HGW* equations are derived by the truncation of high-order connected correlators, whereas the *GW* equations are based on simplification of Hedin's vertex. The comparison of these two sets of equations is summarized in Table I. These formulas will be used to calculate the one-body Green's functions and the particle density in Sec. IV. Now we turn to more complicated many-body correlators.

III. COVARIANT *HGW* APPROXIMATION FOR THE TWO-BODY CORRELATOR

In this section, the covariant scheme is employed for two-body correlators within the *HGW* approximation. The covariant *HGW* equations for the density-density correlators are also derived by functional derivatives of the *HGW* equations.

A. Ward identities and covariance

In a many-body system, the charge conservation leads to a set of the Ward identities (see Appendix A2). In an approximation (such as *GW* or FLEX), the Ward identity for the one-body Green's function is obeyed, whereas the Ward identity for the two-body correlator (directly obtained from equations after the approximation) is often violated. The relation between the charge correlator and charge susceptibility, $\partial n/\partial \mu = \chi^{\mathrm{ch}}(q = 0, \omega = 0)$, is also often violated. To preserve the consistency in the *HGW* approximation, one can define the two-body (connected) correlator as the functional derivative of Green's function G with respect to the external source ϕ:

$$
L^{\mathrm{cov}}(1,2;3) = \left. \frac{\delta G(1,2)}{\delta \phi(3)} \right|_{\phi=0}.
\tag{13}
$$

Here G is obtained from the of-shell (nonzero ϕ) equations. The superscript cov in L^{cov} denotes covariant.

As G obeys the Ward identity for all ϕ's, the derivative of the Ward identity is also satisfied:

$$\int d(2) \left(T(1,2) \frac{\delta G(2,1)}{\delta \phi(3)} - T(2,1) \frac{\delta G(1,2)}{\delta \phi(3)} \right) = 0. \quad (14)$$

Letting $\phi = 0$ in Eq. (14), one obtains

$$\int d(2) \left(T(1,2) L^{\text{cov}}(2,1;3) - T(2,1) L^{\text{cov}}(1,2;3) \right) = 0. \quad (15)$$

Thus one arrives at the conclusion that L^{cov} defined by Eq. (13) satisfies the Ward identity for the two-body correlator. In other words, the covariant scheme automatically preserves all the charge-conserving laws.

B. Covariant HGW equations for the density-density correlator

The covariant version of the density-density correlator is defined as

$$\chi^{\text{cov}}(1,2) = \left. \frac{\delta \rho(1)}{\delta \phi(2)} \right|_{\phi=0}, \quad (16)$$

with ρ the density obtained from of-shell HGW Eqs. (12). To compute χ^{cov}, one differentiates the HGW equations with respect to ϕ. After calculation, given in Appendix B2, one obtains

$$\chi^{\text{cov}}(1,2) = \chi_0(1,2) - \int d(34) \, \chi_0(1,3) V(3,4) \chi^{\text{cov}}(4,2), \quad (17)$$

where the covariant version of polarization function χ_0 satisfies the equation

$$\chi_0(1,2) = - \int d(34) \, G(1,3) G(4,1) \Lambda(3,4;2). \quad (18)$$

The covariant version of vertex function Λ satisfies a set of linear Eqs. (B18) and (B19) given in Appendix B2.

The calculation procedure for χ^{cov} in the covariant HGW approximation therefore can be summarized as follows. First, one solves the on-shell ($\phi = 0$) HGW Eqs. (12) to obtain H, G, W. Second, one solves Eqs. (B18) and (B19) to obtain Λ. Third, one uses Eq. (18) to calculate χ_0. Finally, one solves Eq. (17) to obtain χ^{cov}. These equations, Eqs. (B18), (B19), (18), and (17), are referred to as the covariant HGW equations.

Let us contrast this with a frequently used RPA formula for χ,

$$\chi^{\text{RPA}}(1,2) = \overline{\chi}(1,2) - \int d(34) \overline{\chi}(1,3) V(3,4) \chi^{\text{RPA}}(4,2), \quad (19)$$

where the Lindhard polarization function $\bar{\chi}$ is given by

$$\overline{\chi}(1,2) = -G(1,2) G(2,1), \quad (20)$$

with $G(1,2)$ approximated within a certain approach (such as the GW). Although the RPA scheme is much simpler than the covariant scheme, it does not guarantee the Ward identities. In addition, the charge susceptibility (charge susceptibility) $\partial n / \partial \mu$ is not consistent with that obtained from the RPA

calculation [27]. In contrast, the covariant scheme preserves all these identities.

IV. COMPARISON WITH OTHER APPROXIMATIONS IN THE 2D HUBBARD MODEL

In this section, the HGW approximation is tested on a (numerically) solvable model, the 2D one-band Hubbard model. Exact diagonalization is possible on a relatively small cluster $N \times N$, $N = 4$, so we mainly focus on this system. In many cases, we use determinantal MC in the range of parameters in which it is consistent with the ED (practically, not too low temperature and not too large U).

The discretized time Matsubara action is employed for numerical implementation to the 2D Hubbard model. Results of the Green's function (and the density) within the HGW approximation and the charge correlator (and charge susceptibility) based on the covariant scheme are presented. At any stage, the HGW method is compared to two other relatively simple analytic approaches, GW and FLEX (generally, all three approximations are much better than the HF approximation not shown here).

A. Matsubara action for the 2D Hubbard model

The Hamiltonian of the 2D Hubbard model is

$$\hat{\mathcal{H}} = \sum_{ij} \sum_{\sigma=\uparrow,\downarrow} t_{ij} \hat{\psi}_{i,\sigma}^\dagger \hat{\psi}_{j,\sigma} + U \sum_i \hat{\psi}_{i\uparrow}^\dagger \hat{\psi}_{i\uparrow} \hat{\psi}_{i\downarrow}^\dagger \hat{\psi}_{i\downarrow}$$
$$- \mu \sum_{i,\sigma} \hat{\psi}_{i,\sigma}^\dagger \hat{\psi}_{i,\sigma}. \quad (21)$$

Here $\hat{\psi}_{i\sigma}^\dagger$, $\hat{\psi}_{i\sigma}$ are the creation and annihilation operators of electrons with spin $\sigma = \uparrow, \downarrow$ on lattice site i. The labels i, j denote the coordinates on the $N \times N$ 2D square lattice with periodic boundary conditions (and lattice constant setting the unit of length). The hopping strength t_{ij} equals $-t$, if sites i, j are nearest neighbors and 0 otherwise. We set $t = 1$ to the unit of energy. Coupling U is the on-site repulsion and μ is the chemical potential.

The discretized time Matsubara action [31] for Hamiltonian Eq. (21) has the form

$$S_M[\psi, \psi^*] = \sum_{l=0}^{M-1} \sum_{\sigma=\uparrow,\downarrow} \sum_i \psi_{i\sigma}^*(\tau_l)[\psi_{i\sigma}(\tau_{l+1}) - \psi_{i\sigma}(\tau_l)]$$
$$+ \Delta\tau \sum_{l=0}^{M-1} \mathcal{H}[\psi_{i\sigma}^*(\tau_l), \psi_{i\sigma}(\tau_l)]. \quad (22)$$

Here M is the number of Matsubara time slices, so $\Delta\tau \equiv \beta/M$ is the time step. The discrete label l takes integral value in $[0, M-1]$ and $\tau_l \equiv l\Delta\tau$. The functional $\mathcal{H}$ is obtained by substituting $\psi_{i\sigma}^*(\tau_l), \psi_{i\sigma}(\tau_l)$ for $\hat{\psi}_{i\sigma}^\dagger, \hat{\psi}_{i\sigma}$ in Hamiltonian $\hat{\mathcal{H}}$, respectively.

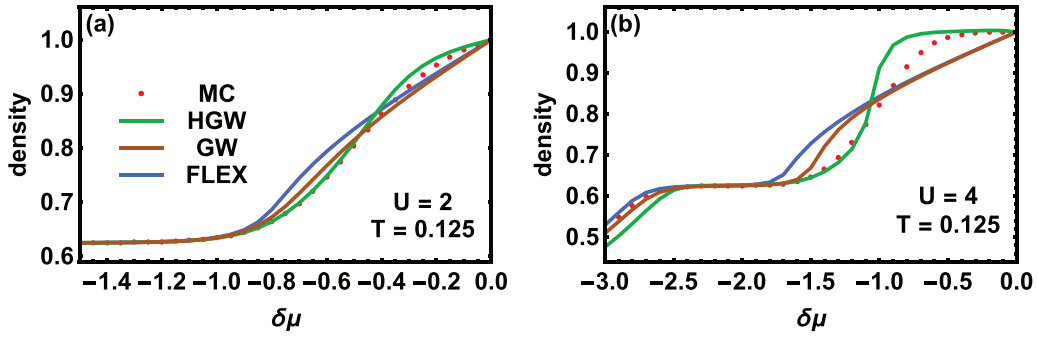Comparing the Matsubara action Eq. (22) with general action Eq. (1), one obtains the expression for the hopping

FIG. 1. The doping $\delta\mu$ dependence of the particle density at (a) $U = 2$, $T = 0.125$ and (b) $U = 4$, $T = 0.125$ for the 4×4 Hubbard cluster. The red dots denote the results obtained from MC. The darker green line denotes the results obtained from HGW equations. The darker orange line denotes the results obtained from GW equations. The royal blue line denotes the results obtained from FLEX approximation.

matrix T,

$$T(1, 2) = \Delta\tau\delta_{\sigma_1\sigma_2}\left(-\frac{1}{\Delta\tau}\delta_{i_1i_2}\big(\delta_{l_1,l_2-1} - \delta_{l_1,l_2}\big) - t_{i_1i_2}\delta_{l_1l_2} + \mu\delta_{i_1i_2}\delta_{l_1l_2}\right), \tag{23}$$

and the expression for the two-body interaction potential V,

$$V(1, 2) = \Delta\tau U\delta_{\sigma_1\overline{\sigma_2}}\delta_{l_1l_2}\delta_{i_1i_2}, \tag{24}$$

where Eq. (1) denotes $(\sigma_1, i_1, \tau_{l_1})$, which is a collection of the spin, the lattice coordinate, and the Matsubara time indexes. Here the symbol $\overline{\sigma}$ means the flip of the spin σ. The correlators in discretized time Matsubara action are discussed in Appendix D.

For a given set of parameters $U, \mu, T \equiv 1/\beta$ (and N, M), one solves the HGW Eqs. (12) to obtain the Green's functions. The HGW equations in frequency-momentum space are given in Appendix C2, the covariant HGW equations in frequency-momentum space are given in Appendix C3, and the numerical algorithm and cost are described in Appendix E. We start with the thermodynamics and then proceed to the Matsubara Green's function and the charge correlator.

B. Doping dependence of the particle density

To study the doping dependence of the particle density, we chose $T = 0.125$ for 4×4 cluster and two values of the on-site repulsion $U = 2$, representing the weak coupling strength, see Fig. 1(a) and $U = 4$, representing the intermediate coupling strength, see Fig. 1(b). The results are compared with those obtained from GW, FLEX, and determinantal MC (the ED approach produces numerically the same results). In Fig. 1(a), the three curves are all close to the MC result (dots), which means HGW, GW, and FLEX all produce satisfactory results of the density at weak coupling regime. In Fig. 1(b), the HGW curve is much closer to MC result than GW and FLEX when the particle density is larger than 0.6, which shows HGW is much better than GW and FLEX in the strong antiferromagnetic fluctuation regime. In addition, MC dots show a plateau resembling the Mott-Hubbard gap (due to the strong antiferromagnetic fluctuation) phase near half filling. The HGW curve exhibits

this property, whereas GW and FLEX fail. In this degree, the HGW approximation has the advantage of capturing the Mott-Hubbard gap over the GW and FLEX approximations.

C. Matsubara Green's function

1. Matsubara Green's function at the Matsubara time axis

We compare results of Green's function at the Matsubara time axis at the antinodal momentum $k = (\pi, 0)$ and the nodal point $k = (\pi/2, \pi/2)$ (see Fig. 2) for different doping and the coupling strength with $T = 0.125$ for the 4×4 cluster. At $U = 2$ and half filling [see Figs. 2(a) and 2(e)], the GW and FLEX curves are close to the MC data (dots), whereas the HGW curve is relatively further. At $U = 2$ and away from half filling [see Figs. 2(b) and 2(f)], the three curves are close to each other, but all relatively further away from the MC result. These results demonstrate that HGW might not be advantageous in the weak coupling regime (particularly at half filling).

At a stronger coupling $U = 4$, at half filling [see Figs. 2(c) and 2(g)], the HGW curve is much closer to the MC than the GW and the FLEX curves. As away from half filling [see Figs. 2(d) and 2(h)], the HGW curve is also much closer to the MC data than the GW and FLEX curves. These results demonstrate that the HGW approximation has a considerable advantage over GW and FLEX in the strong coupling regime, especially away from half filling.

At half filling, the determinantal MC is applicable to an 8×8 lattice. We compare the HGW method in these cases (see Fig. 3). These results also demonstrate that at $U = 2$, the HGW method is worse than the GW and FLEX methods, but is better at $U = 4$.

These results can be understood as follows. The HGW approximation is obtained by truncating the three-body connected correlators, which have a good clustering property at a stronger coupling U. At $U = 2$, the three-body connected
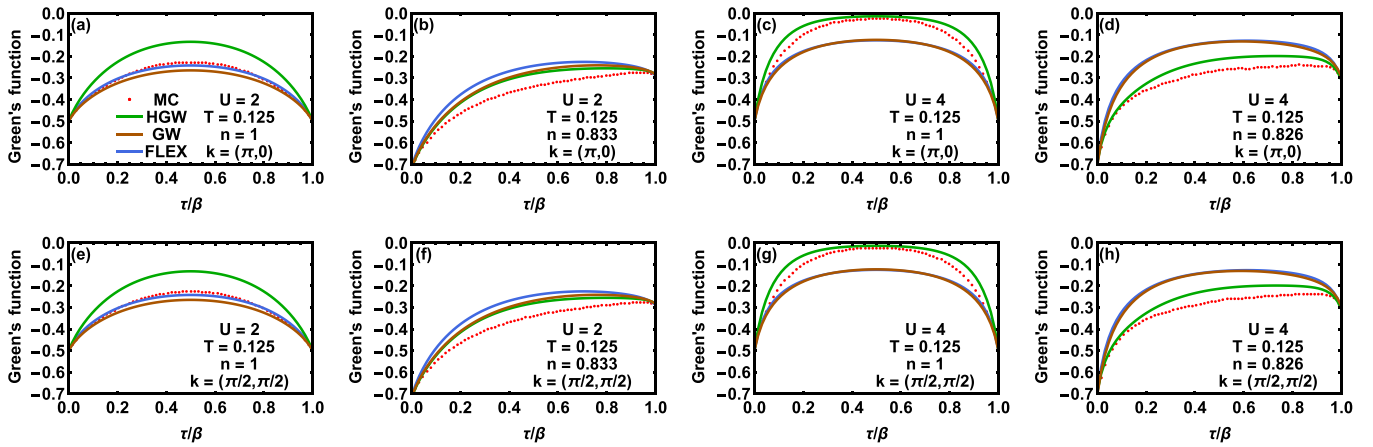
FIG. 2. Comparison of results of Green's function at Matsubara time axis for 4×4 cluster at $T = 0.125$ for different parameters: (a) $U = 2, n = 1, k = (\pi, 0)$, (b) $U = 2, n = 0.833, k = (\pi, 0)$, (c) $U = 4, n = 1, k = (\pi, 0)$, (d) $U = 4, n = 0.826, k = (\pi, 0)$, (e) $U = 2, n = 1, k = (\pi/2, \pi/2)$, (f) $U = 2, n = 0.833, k = (\pi/2, \pi/2)$, (g) $U = 4, n = 1, k = (\pi/2, \pi/2)$, (h) $U = 4, n = 0.826, k = (\pi/2, \pi/2)$. The red dots denote the results obtained from MC. The darker green line denotes the results obtained from the HGW equations. The darker orange line denotes the results obtained from the GW equations. Royal blue line denotes the results obtained from the FLEX approximation.

correlators might be very nonlocal and the inequality Eq. (10) does not hold and, as a result, the HGW method doesn't perform so well. In contrast, at $U = 4$, the connected correlators become local and the HGW method exhibits its advantage.

2. Spectral function at half filling

Using the discrete Fourier transformation, one obtains the values of the Green's function at small Matsubara frequencies from those at Matsubara time axis. The comparison of the
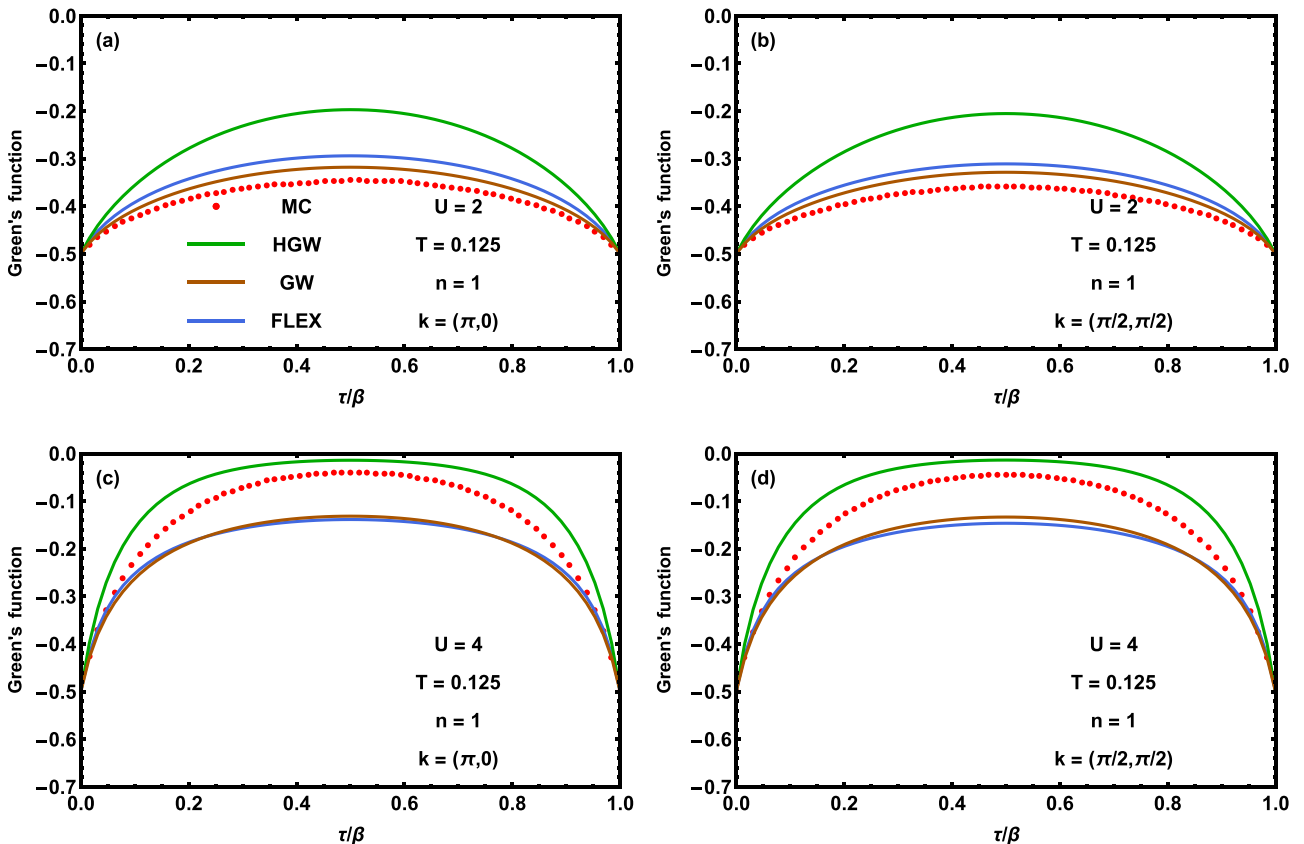

FIG. 3. Comparison of results of Green's function at Matsubara time axis for 8×8 cluster for different parameters: (a) $U = 2, T = 0.125, n = 1, k = (\pi, 0)$, (b) $U = 2, T = 0.125, n = 1, k = (\pi/2, \pi/2)$, (c) $U = 4, T = 0.125, n = 1, k = (\pi, 0)$, (d) $U = 4, T = 0.125, n = 1, k = (\pi/2, \pi/2)$. The red dots denote the results obtained from determinantal MC. The darker green line denotes the results obtained from HGW equations. The darker orange line denotes the results obtained from GW equations. The royal blue line denotes the results obtained from FLEX approximation.
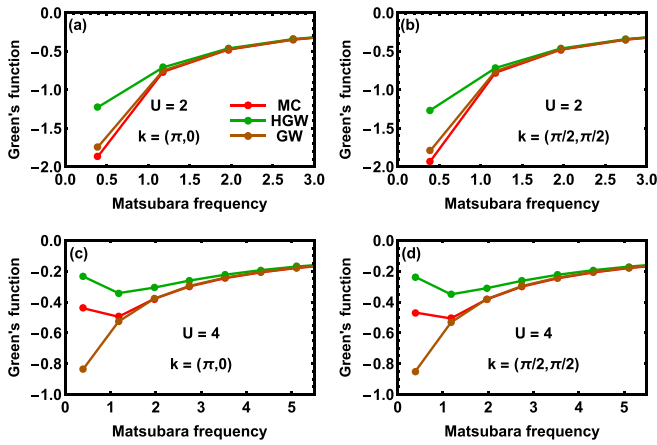
FIG. 4. Comparison of the results of the imaginary part of the Green's function at the Matsubara frequency axis for an 8×8 cluster for different parameters: (a) $U = 2, T = 0.125, n = 1, k = (\pi, 0)$, (b) $U = 2, T = 0.125, n = 1, k = (\pi/2, \pi/2)$, (c) $U = 4, T = 0.125, n = 1, k = (\pi, 0)$, (d) $U = 4, T = 0.125, n = 1, k = (\pi/2, \pi/2)$. The red dots denote the results obtained from determinantal MC. The darker green line denotes the results obtained from *HGW* equations. The darker orange line denotes the results obtained from *GW* equations.

imaginary part of the value of the Green's function at the Matsubara frequency axis at half filling for an 8×8 cluster is shown in Fig. 4. These results demonstrate again that the *HGW* method is worse than the traditional *GW* method in the weak coupling regime. At a stronger coupling, $U = 4$, the shape of the *HGW* curve implies a Mott-Hubbard gap, just like the MC curve. On the contrary, the *GW* method fails.

With the values of the Green's function at some Matsubara frequencies, one can obtain the spectral function by the analytical continuation. We adopt the Nevanlinna analytical continuation [32], which is applicable to noiseless Matsubara data. The results of the spectral function at $U = 4, T = 0.125$ at half filling for the 8×8 cluster are shown in Fig. 5. The spectral function obtained from the *HGW* method does exhibit a Mott-Hubbard gap. The spectral function for the 2D half-

filling Hubbard model has been studied by various methods, for example, the MC simulation [33], the ladder dual fermion approximation [34], the cellular dynamical mean-field theory [35], and the cluster perturbation theory [36]. We found that our results are similar to those obtained by the cluster perturbation theory (Fig. 9(c) presented in Ref. [34]).

D. Charge density correlator and charge susceptibility at half filling

We compare the charge correlator in Matsubara time at the quasimomentum (π, π) obtained from the covariant *HGW* approximation (c*HGW*) with those based on the RPA formula (19), (20), where the Green's functions G obtained from the *HGW, GW*, FLEX approximations are used.

We study the 4×4 cluster and set $M = 1024$. Two sets of parameters are chosen: $U = 2, T = 0.125$ in Figs. 6(a) and 6(b), and $U = 4, T = 0.125$ in Figs. 6(c) and 6(d). Since the results turn out to be too close to differentiate, only the FLEX and MC curves for the charge correlator are plotted in Figs. 6(a) and 6(c), and the differences between the results obtained from the above approximations and those obtained from MC are plotted in Figs. 6(b) and 6(d).

In Fig. 6(b), with parameter $U = 2, T = 0.125$, the largest differences given by *HGW, GW*, and FLEX (within the RPA formula) are all about 0.12 (near $\tau = 0$ and $\tau = \beta$), while that given by c*HGW* is about 0.01. In Fig. 6(d), with parameter $U = 4, T = 0.125$, the largest differences (near $\tau = 0$ and $\tau = \beta$) given by *HGW, GW*, and FLEX are all about 0.15, while that given by c*HGW* is less than 0.01. These results demonstrate that the covariant scheme makes a significant improvement over the RPA calculations.

We study the dependence of the static charge susceptibility $\chi^{\text{ch}}(i\Omega = 0, k)$ on the coupling strength U at $T = 0.125$, and these results are presented in Figs. 7(a) and 7(b). The curves obtained from the c*HGW* method and the RPA calculations with the Green's function obtained from the *HGW, GW*, and FLEX approximations have a similar tendency to the MC curve. The c*HGW* curve is much closer to the MC curve, which demonstrates again that the covariant scheme makes a significant improvement over the RPA calculations.
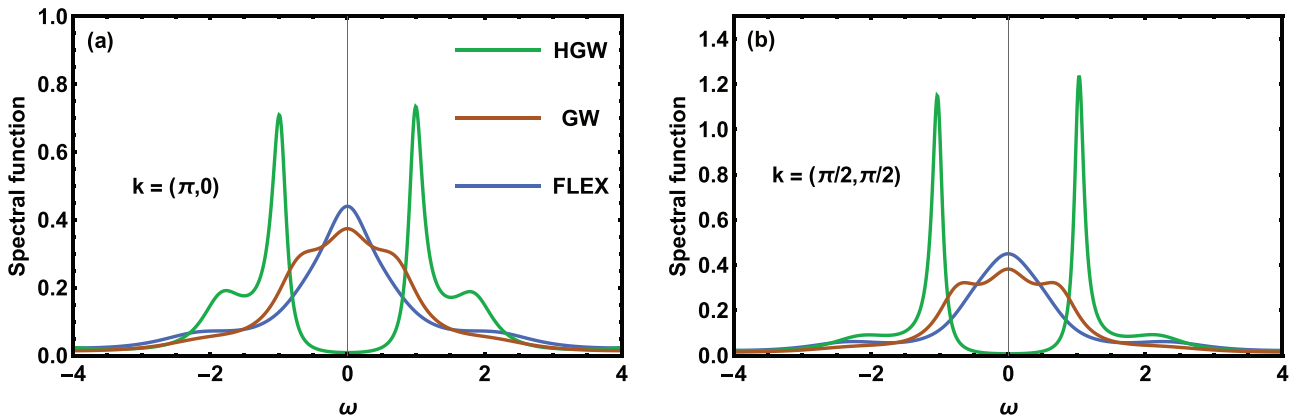

FIG. 5. Comparison of the results of the spectral functions for 8×8 cluster at $U = 4, T = 0.125$ and half filling at different momenta: (a) $k = (\pi, 0)$, (b) $k = (\pi/2, \pi/2)$. The darker green line denotes for the results of the spectral function obtained from the *HGW* method, the darker orange line denotes those obtained from the *GW* method, and the royal blue line denotes those obtained from the FLEX theory.
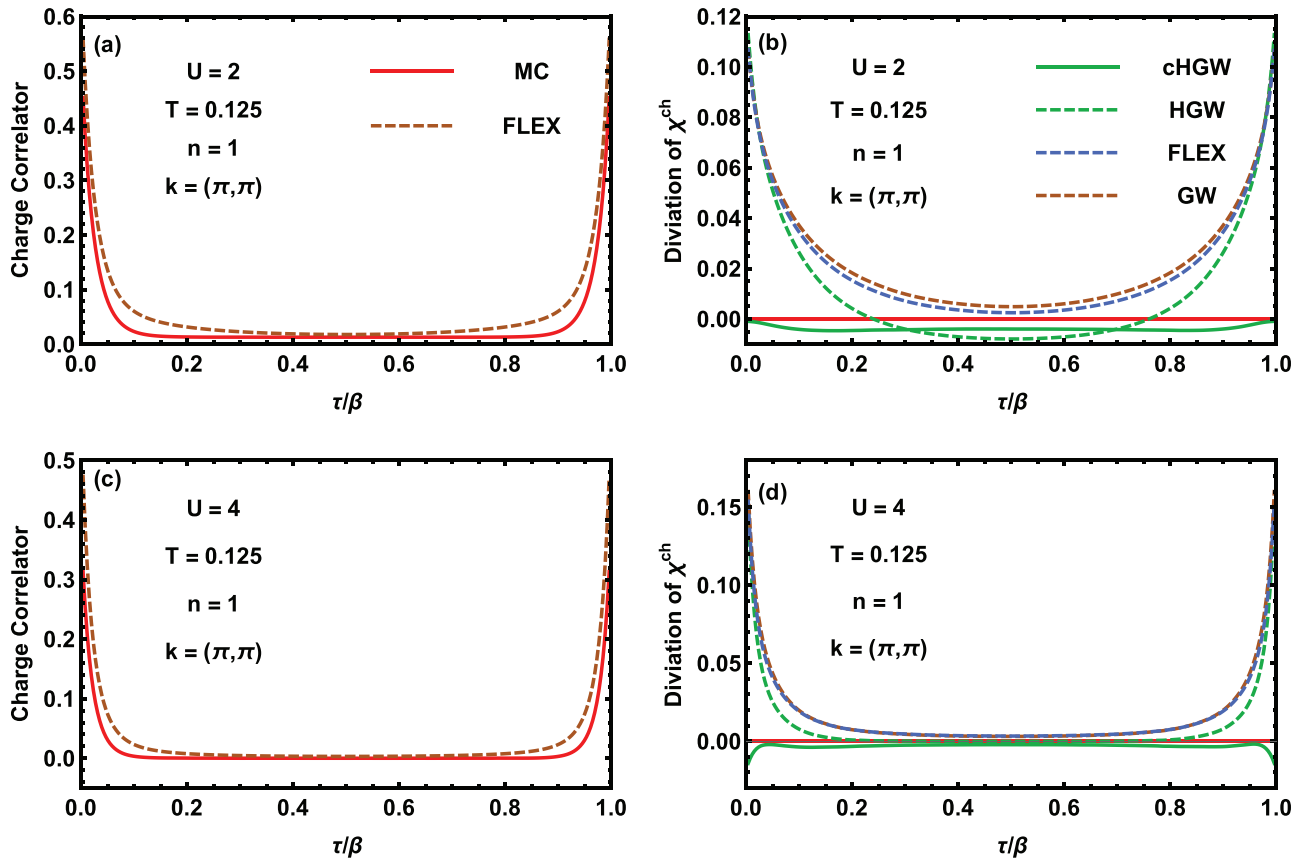
FIG. 6. Comparison of results of charge correlator in Matsubara time at $k = (\pi, \pi)$ the 4×4 Hubbard cluster. For $U = 2$, $T = 0.125$, $n = 1$, (a) shows the results of charge correlator obtained from FLEX and MC and (b) shows the differences between results of charge correlator obtained from different approximations and those obtained from MC. For $U = 4$, $T = 0.125$, $n = 1$, (c) shows the results of charge correlator and (d) shows the differences. The red line denotes MC. The darker green solid line denotes $cHGW$ and the darker green dashed line denotes HGW. The darker orange dashed line denotes GW. The royal blue dashed line denotes FLEX.

We also compare the values of $\partial n / \partial \mu$ (by variation of the density with the chemical potential, i.e., $\Delta n / \Delta \mu$) at different couplings and the results are presented in Fig. 7(c). The HGW curve is much closer to the MC curve than the GW and FLEX curves. The tendency of $\partial n / \partial \mu$ to 0 as U increases showed by the MC results demonstrates the Mott-Hubbard gap at strong coupling.

In a self-consistent theory, the static charge susceptibility $\chi_c \equiv \chi^{ch}(i\Omega = 0, k = 0)$ is equal to the quantity $\partial n / \partial \mu$ from an independent calculation. To study this consistency, we compare the quantity $\partial n / \partial \mu - \chi_c$, and the results are presented in Fig. 7(d). The results demonstrate that the MC and the covariant calculations hold the consistency, whereas the RPA calculations have significant deviations.

V. CONCLUSION AND DISCUSSION

To summarize, the HGW approximation, a modified GW approximation, is developed. It is derived by introduction of an external source ϕ coupled to the density ρ and truncation of high-order correlators on equations of motion. The complexity of the HGW equations turn out to be very similar to GW equations. The HGW approximation is compared with other approximations of comparable complexity GW, FLEX in the Hubbard model. The results of the density and

Green's function demonstrate that the HGW approximation has a significant advantage over GW and FLEX in a relative strong coupling regime especially away from half filling. More importantly, the HGW approximation exhibits a gap as U increases, whereas the GW and FLEX methods fail.

To obtain the charge-conserving two-body correlators in the HGW approximation, the covariant scheme is developed. In this scheme, the two-body correlators are calculated through functional derivatives of Green's function G with respect to the source ϕ. The covariant scheme for the charge correlator is compared with the RPA scheme and determinantal MC in the Hubbard model. The comparison demonstrates that the covariant scheme makes a significant improvement over the RPA scheme. The comparison of charge susceptibility demonstrates that the covariant scheme for the charge correlator is consistent with the charge susceptibility, whereas the RPA calculation has a significant deviation.

The HGW method (to calculate the one-body Green's function) has a small complexity (for details, see Appendix E), and thus can be applied to large systems. The formalism presented in this paper is easily extended to more general cases, such as multiorbital lattice models, as long as the band index is put in the generalized coordinate. The similarity to the traditional GW method helps the application of the HGW method to study the electronic properties of realistic
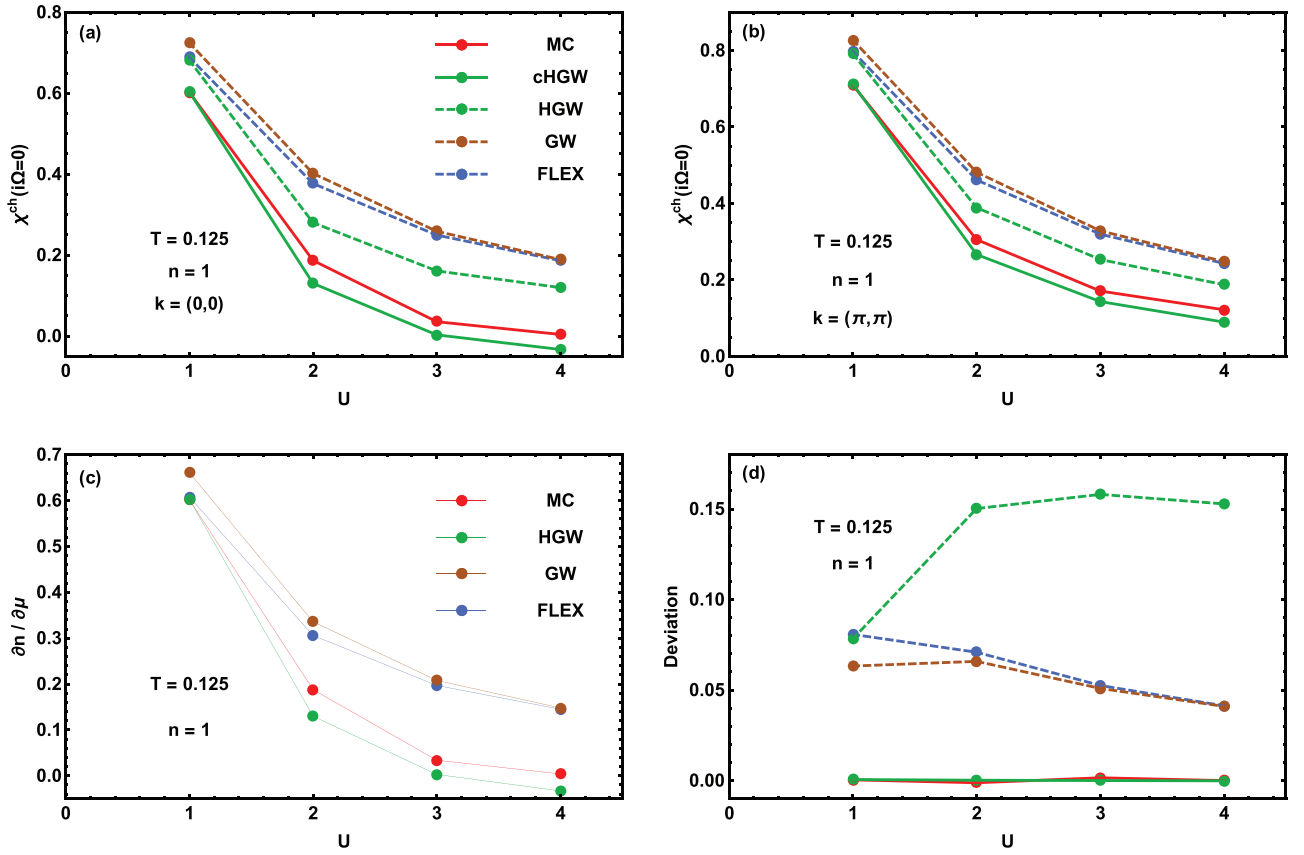
FIG. 7. Comparison of the results of the static charge susceptibility dependence of U at $T = 0.125$ for the 4×4 Hubbard cluster. (a) shows the results of the static charge susceptibility obtained from the MC, cHGW, HGW, GW, FLEX methods, at $k = (0, 0)$, (b) at $k = (\pi, \pi)$. (c) shows the values of $\partial n / \partial \mu$ obtained from the independent calculations through MC, HGW, GW, and FLEX methods. (d) shows the deviation of the RPA calculations. In (a), (b), and (d), the red line denotes MC, the darker green solid line denotes cHGW, the darker green dashed line denotes HGW, the darker orange dashed line denotes GW, and the royal blue dashed line denotes FLEX. In (c), the red line denotes MC, the darker green solid line denotes HGW, the darker orange solid line denotes GW, and the royal blue solid line denotes FLEX.

correlated materials. The substantial improvement over the GW method in the relatively strong coupling regime might imply that the HGW method is a good alternative in certain cases. However, the numerical cost of the calculation of the charge-conserving charge correlators is too large for realistic systems.

To fully study the Hubbard model, the spin channel is important, whereas it is neglected in our current formalism (the traditional GW method also neglects the spin channel). The variants of the GW method including spin channel were proposed, for example, in Refs. [37–39]. A variant of the HGW approximation could also be proposed by including spin channel to better account the spin fluctuation at the strong fluctuation regime in the 2D Hubbard model in future research.

The self-consistency is important to nonperturbative analytical methods, and numerous ideas are put forward to ensure several identities. For example, in the two-particle self-consistent theory [40–42], several constants are determined by the sum rules and identities. In contrast, the idea of the covariance is natural and universal in a sense that the correlators and the sum rules are treated in the same footing.

APPENDIX A: DYSON-SCHWINGER EQUATIONS AND WARD IDENTITIES

1. Dyson-Schwinger equations of motion

The invariance of the functional integral measure $\mathcal{D}[\psi, \psi^*]$ under the infinitesimal variation of field ψ, ψ^* yields the equality [43]

$$\int \mathcal{D}[\psi, \psi^*] \frac{\delta}{\delta \psi^*(2)} \left(\psi^*(1) e^{-S[\psi, \psi^*; \phi]} \right) = 0. \quad \text{(A1)}$$

Substituting the perturbed action Eq. (2) into the equality, one obtains the Dyson-Schwinger equation of motion:

$$\delta(1,2) = \int d(3)\, T(1,3)G(3,2) + \phi(1)G(1,2)$$
$$- \int d(3)\, V(1,3)G_2(1,2;3,3). \quad (A2)$$

Here the two-body correlator is defined by

$$G_2(1,2;3,4) \equiv \langle \psi^*(2)\psi(1)\psi^*(4)\psi(3) \rangle$$
$$= \frac{1}{Z[\phi]} \int \mathcal{D}[\psi,\psi^*]\, \psi^*(2)\psi(1)\psi^*(4)\psi(3)$$
$$\times\, e^{-S[\psi,\psi^*;\phi]}. \quad (A3)$$

Through the definition Eq. (4), one obtains the derivative of G with respect to ϕ,

$$L(1,2;3) \equiv \frac{\delta G(1,2)}{\delta\phi(3)} = G_2(1,2;3,3) - G(1,2)\rho(3), \quad (A4)$$

where $\rho(1) \equiv \langle \rho(1) \rangle = G(1,1)$. By virtue of Eq. (A4), one can express G_2 in terms of G and $\delta G/\delta\phi$, and thus can obtain Eq. (5) from Eq. (A2).

2. Ward identities for correlators

The invariance of the functional integral measure $\mathcal{D}[\psi,\psi^*]$ under the infinitesimal phase rotation of the complex field ψ yields an equality [43]

$$\int \mathcal{D}[\psi,\psi^*] \left(\psi^*(1)\frac{\delta}{\delta\psi^*(1)} - \psi(1)\frac{\delta}{\delta\psi(1)} \right) e^{-S[\psi,\psi^*;\phi]} = 0. \quad (A5)$$

Substituting the perturbed action Eq. (2), one obtains the Ward identity for Green's function G:

$$\int d(2)\, T(1,2)G(2,1) - T(2,1)G(1,2) = 0. \quad (A6)$$

The derivative of Eq. (A6) with respect to ϕ yields

$$\int d(2)\, T(1,2)L(2,1;3) - T(2,1)L(1,2;3) = 0. \quad (A7)$$

Equation (A7) is the Ward identity for the two-body correlator L.

APPENDIX B: DETAILS OF DERIVING HGW EQUATIONS AND COVARIANT HGW EQUATIONS

1. Derivation of HGW equations

The HGW equations are derived from Eqs. (5) and (11). First, one makes a derivative of Eqs. (6) and (7) with respect to ϕ, and obtains

$$\frac{\delta H^{-1}(1,2)}{\delta\phi(3)} = \delta(1,2)\frac{\delta v(1)}{\delta\phi(3)} \quad (B1)$$

and

$$\frac{\delta v(1)}{\delta\phi(2)} = \delta(1,2) - \int d(3)\, V(1,3)\frac{\delta\rho(3)}{\delta\phi(2)}. \quad (B2)$$

Substituting Eq. (B1) into Eq. (11) leads to

$$\frac{\delta G(1,2)}{\delta\phi(3)} = -\int d(4)\, H(1,4)G(4,2)\frac{\delta v(4)}{\delta\phi(3)}. \quad (B3)$$

Plugging Eq. (B3) into Eq. (B2), one obtains

$$\frac{\delta v(1)}{\delta\phi(2)} = \delta(1,2) + \int d(34)\, V(1,3)\Pi(3,4)\frac{\delta v(4)}{\delta\phi(2)}, \quad (B4)$$

with

$$\Pi(1,2) \equiv H(1,2)G(2,1). \quad (B5)$$

Then substituting Eq. (B3) into Eq. (5), one obtains

$$\delta(1,2) = \int d(3)\, H^{-1}(1,3)G(3,2)$$
$$+ \int d(34)\, V(1,3)H(1,4)G(4,2)\frac{\delta v(4)}{\delta\phi(3)}. \quad (B6)$$

The equation above can be rewritten as

$$G^{-1}(1,2) = H^{-1}(1,2) - \Sigma(1,2), \quad (B7)$$

with the self-energy function Σ given by

$$\Sigma(1,2) \equiv -H(1,2)W(2,1), \quad (B8)$$

and the screened dynamical potential W defined by

$$W(1,2) \equiv \int d(3)\, \frac{\delta v(1)}{\delta\phi(3)}V(2,3). \quad (B9)$$

Combining Eqs. (B4) and (B9), one arrives at the following equation:

$$W(1,2) = V(1,2) + \int d(34)\, V(1,3)\Pi(3,4)W(4,2), \quad (B10)$$

which can be rewritten as

$$W^{-1}(1,2) = V^{-1}(1,2) - \Pi(1,2). \quad (B11)$$

Now four important equations [Eqs. (B5), (B7), (B8), and (B11)] are derived and they are called the HGW equations.

2. Derivation of covariant HGW equations

Here, details of derivation of covariant HGW equations are given. For convenience, one can introduce the covariant versions of two vertex functions:

$$\Lambda(1,2;3) \equiv \left. \frac{\delta G^{-1}(1,2)}{\delta v(3)} \right|_{\phi=0} \quad (B12)$$

and

$$\Gamma(1,2;3) \equiv \left. \frac{\delta W^{-1}(1,2)}{\delta v(3)} \right|_{\phi=0}. \quad (B13)$$

The derivatives of HGW equations with respect to v can be easily obtained:

$$\Lambda(1,2;3) = \frac{\delta H^{-1}(1,2)}{\delta v(3)} + \frac{\delta H(1,2)}{\delta v(3)}W(2,1)$$
$$+ H(1,2)\frac{\delta W(2,1)}{\delta v(3)}, \quad (B14)$$

$$\Gamma(1,2;3) = -\frac{\delta H(1,2)}{\delta v(3)}G(2,1) - H(1,2)\frac{\delta G(2,1)}{\delta v(3)}. \quad (B15)$$

There is a general relation for an array X,

$$\frac{\delta X(1, 2)}{\delta v(3)} = -\int d(45)\, X(1, 4)X(5, 2)\frac{\delta X^{-1}(4, 5)}{\delta v(3)}, \quad \text{(B16)}$$

and for $X = H$,

$$\frac{\delta H^{-1}(1, 2)}{\delta v(3)} = \delta(1, 2)\delta(1, 3). \quad \text{(B17)}$$

Then one can obtain the equation for Λ,

$$\Lambda(1, 2; 3) = \delta(1, 2)\delta(1, 3) - H(1, 3)H(3, 2)W(2, 1)$$
$$- \int d(45)\, H(1, 2)W(2, 5)W(4, 1)\Gamma(5, 4; 3), \quad \text{(B18)}$$

and the equation for Γ:

$$\Gamma(1, 2; 3) = H(1, 3)H(3, 2)G(2, 1)$$
$$+ \int d(45)\, H(1, 2)G(2, 5)G(4, 1)\Lambda(5, 4; 3). \quad \text{(B19)}$$

From Eqs. (B18) and (B19), one can obtain Λ and Γ, giving H, G, W obtained from on-shell ($\phi = 0$) HGW equations.

One can introduce χ_0 as

$$\chi_0(1, 2) \equiv \left.\frac{\delta\rho(1)}{\delta v(2)}\right|_{\phi=0}, \quad \text{(B20)}$$

and then obtain Eq. (18). With the definitions Eqs. (16) and (B20), one obtains

$$\chi^{\text{cov}}(1, 2) = \int d(3)\, \chi_0(1, 3)\frac{\delta v(3)}{\delta\phi(2)}. \quad \text{(B21)}$$

By virtue of Eq. (B2), Eq. (B21) leads to Eq. (17).

APPENDIX C: *HGW* AND COVARIANT *HGW* EQUATIONS FOR THE HUBBARD MODEL

1. Generalized Fourier transformation for the Hubbard model

The generalized Fourier transformation for the Hubbard model is introduced here. For a short formulation, two useful notations,

$$\mathcal{E}_{\text{F}}(\alpha, 1 - 2) \equiv e^{\mathrm{i}\pi\eta_\alpha\cdot(\sigma_1-\sigma_2)}e^{\mathrm{i}\,k_\alpha\cdot(i_1-i_2)}e^{\mathrm{i}\pi(2m_\alpha+1)\cdot(\tau_1-\tau_2)}, \quad \text{(C1)}$$

$$\mathcal{E}_{\text{B}}(\alpha, 1 - 2) \equiv e^{\mathrm{i}\pi\eta_\alpha\cdot(\sigma_1-\sigma_2)}e^{\mathrm{i}\,k_\alpha\cdot(i_1-i_2)}e^{\mathrm{i}\pi 2m_\alpha\cdot(\tau_1-\tau_2)}, \quad \text{(C2)}$$

are introduced, where label α refers to $\eta_\alpha, k_\alpha, m_\alpha$. For a fermionic array X_{F} which is antiperiodic over Matsubara time, one can expand it as Fourier series:

$$X_{\text{F}}(1, 2) = \frac{1}{\mathcal{N}}\sum_\alpha \tilde{X}_{\text{F}}(\alpha)\mathcal{E}_{\text{F}}(\alpha, 1 - 2). \quad \text{(C3)}$$

Here $\mathcal{N} = 2MN^2$, M is the number of time slices and N^2 is the number of lattice sites. σ is quantified as 1 for spin down and 0 for spin up and, correspondingly, η takes value of 0 or 1. i is the coordinate of lattice site and k is the momentum in the first Brillouin zone. $\tau \in [0, \beta]$ is the discrete Matsubara time and m takes integral value from 0 to $M - 1$. The summation $\sum_\alpha$ is over all possible values of $\alpha \equiv (\eta_\alpha, k_\alpha, m_\alpha)$. Similarly,

one can expand a bosonic array X_{B}, which is periodic over Matsubara time, as a Fourier series:

$$X_{\text{B}}(1, 2) = \frac{1}{\mathcal{N}}\sum_\alpha \tilde{X}_{\text{B}}(\alpha)\mathcal{E}_{\text{B}}(\alpha, 1 - 2). \quad \text{(C4)}$$

The coefficient T in action Eq. (1) is antiperiodic over Matsubara time and thus is a fermionic array. Substitute Eq. (23) into the ansatz Eq. (C3), and one obtains

$$\tilde{T}(\alpha) = \Delta\tau\left(-\frac{1}{\Delta\tau}(e^{-\mathrm{i}\pi(2m+1)/M} - 1) - \varepsilon(k_\alpha) + \mu\right), \quad \text{(C5)}$$

with

$$\varepsilon(k) = -2t(\cos(k_x) + \cos(k_y)) \quad \text{(C6)}$$

for the 2D Hubbard model, with $k \equiv (k_x, k_y)$. The coefficient V is periodic over Matsubara time and thus is a bosonic array. Substituting Eq. (24) into the ansatz Eq. (C4), one obtains

$$\tilde{V}(\alpha) = \Delta\tau U(-1)^{\eta_\alpha}. \quad \text{(C7)}$$

From definitions Eqs. (C1) and (C2), one can derive the following relations:

$$\mathcal{E}_{\text{F}}(\alpha, 1 - 2)\mathcal{E}_{\text{F}}(\alpha, 2 - 3) = \mathcal{E}_{\text{F}}(\alpha, 1 - 3),$$
$$\mathcal{E}_{\text{B}}(\alpha, 1 - 2)\mathcal{E}_{\text{B}}(\alpha, 2 - 3) = \mathcal{E}_{\text{B}}(\alpha, 1 - 3),$$
$$\mathcal{E}_{\text{F}}(\alpha, 1 - 2)\mathcal{E}_{\text{B}}(\beta, 1 - 2) = \mathcal{E}_{\text{F}}(\alpha + \beta, 1 - 2),$$
$$\mathcal{E}_{\text{B}}(\alpha, 1 - 2)\mathcal{E}_{\text{B}}(\beta, 1 - 2) = \mathcal{E}_{\text{B}}(\alpha + \beta, 1 - 2),$$
$$\mathcal{E}_{\text{F}}(\alpha, 1 - 2)\mathcal{E}_{\text{F}}(\beta, 2 - 1) = \mathcal{E}_{\text{B}}(\alpha - \beta, 1 - 2),$$
$$\mathcal{E}_{\text{B}}(\alpha, 1 - 2) = \mathcal{E}_{\text{B}}(-\alpha, 2 - 1). \quad \text{(C8)}$$

These equations are helpful in the derivation of HGW equations in Fourier space.

2. *HGW* equations for the Hubbard model

In HGW equations, one encounters several quantities: the fermionic arrays H, G, Σ and the bosonic arrays W, Π. Substitute the ansatz Eqs. (C3) and (C4) into the HGW equations, and one obtains the HGW equations in Fourier space for the Hubbard model:

$$\tilde{G}^{-1}(\alpha) = \tilde{H}^{-1}(\alpha) - \tilde{\Sigma}(\alpha),$$
$$\tilde{\Sigma}(\alpha) = -\frac{1}{\mathcal{N}}\sum_\gamma \tilde{H}(\alpha + \gamma)\tilde{W}(\gamma),$$
$$\tilde{W}^{-1}(\alpha) = \tilde{V}^{-1}(\alpha) - \tilde{\Pi}(\alpha),$$
$$\tilde{\Pi}(\alpha) = \frac{1}{\mathcal{N}}\sum_\gamma \tilde{H}(\alpha + \gamma)\tilde{G}(\gamma), \quad \text{(C9)}$$

with

$$\tilde{H}^{-1}(\alpha) = \tilde{T}(\alpha) - \frac{2U}{\mathcal{N}}\sum_\gamma \tilde{G}(\gamma). \quad \text{(C10)}$$

3. Covariant *HGW* equations for the Hubbard model

Similarly, one can obtain the covariant *HGW* equations in Fourier space for the Hubbard model. One can make the ansatz for the vertex functions:

$$\Lambda(1, 2, 3) = \frac{1}{\mathcal{N}^2} \sum_{\alpha, \gamma} \tilde{\Lambda}(\alpha, \gamma) \mathcal{E}_{\mathrm{F}}(\alpha, 1 - 2) \mathcal{E}_{\mathrm{B}}(\gamma, 1 - 3),$$

$$(C11)$$

$$\Gamma(1, 2, 3) = \frac{1}{\mathcal{N}^2} \sum_{\alpha, \gamma} \tilde{\Gamma}(\alpha, \gamma) \mathcal{E}_{\mathrm{B}}(\alpha, 1 - 2) \mathcal{E}_{\mathrm{B}}(\gamma, 1 - 3).$$

$$(C12)$$

And one can obtain from Eqs. (B18) and (B19),

$$\tilde{\Lambda}(\alpha, \beta) = 1 - \frac{1}{\mathcal{N}} \sum_{\gamma} \tilde{H}(\alpha + \beta + \gamma) \tilde{H}(\alpha + \gamma) \tilde{W}(\gamma)$$

$$- \frac{1}{\mathcal{N}} \sum_{\gamma} \tilde{H}(\alpha + \beta + \gamma) \tilde{W}(\beta + \gamma) \tilde{W}(\gamma) \tilde{\Gamma}(\gamma, \beta)$$

$$(C13)$$

and

$$\tilde{\Gamma}(\alpha, \beta) = \frac{1}{\mathcal{N}} \sum_{\gamma} \tilde{H}(\alpha + \beta + \gamma) \tilde{H}(\alpha + \gamma) \tilde{G}(\gamma)$$

$$+ \frac{1}{\mathcal{N}} \sum_{\gamma} \tilde{H}(\alpha + \beta + \gamma) \tilde{G}(\beta + \gamma) \tilde{G}(\gamma) \tilde{\Lambda}(\gamma, \beta).$$

$$(C14)$$

Combine Eqs. (C13) and (C14), and one obtains

$$\sum_{\gamma} \mathcal{M}(\alpha, \gamma, \beta) \tilde{\Lambda}(\gamma, \beta) = b(\alpha, \beta), \qquad (C15)$$

with

$$\mathcal{M}(\alpha, \gamma, \beta) = \delta(\alpha, \gamma) + \frac{1}{\mathcal{N}} \tilde{G}(\beta + \gamma) \tilde{G}(\gamma)$$

$$\times \frac{1}{\mathcal{N}} \sum_{\lambda} \tilde{H}(\alpha + \beta + \lambda) \tilde{W}(\beta + \lambda) \tilde{W}(\lambda)$$

$$\times \tilde{H}(\beta + \gamma + \lambda) \qquad (C16)$$

and

$$b(\alpha, \beta) = 1 - \frac{1}{\mathcal{N}} \sum_{\gamma} \tilde{H}(\alpha + \beta + \gamma) \tilde{H}(\alpha + \gamma) \tilde{W}(\gamma)$$

$$- \frac{1}{\mathcal{N}} \sum_{\gamma} \tilde{H}(\alpha + \beta + \gamma) \tilde{W}(\beta + \gamma) \tilde{W}(\gamma)$$

$$\times \frac{1}{\mathcal{N}} \sum_{\lambda} \tilde{H}(\beta + \gamma + \lambda) \tilde{H}(\gamma + \lambda) \tilde{G}(\lambda).$$

$$(C17)$$

Once Eq. (C15) is solved, $\tilde{\Lambda}$ will be obtained.

Next, one can make ansatz

$$\chi_0(1, 2) = \frac{1}{\mathcal{N}} \sum_{\alpha} \tilde{\chi}_0(\alpha) \mathcal{E}_{\mathrm{B}}(\alpha, 1 - 2), \qquad (C18)$$

$$\chi^{\mathrm{cov}}(1, 2) = \frac{1}{\mathcal{N}} \sum_{\alpha} \tilde{\chi}^{\mathrm{cov}}(\alpha) \mathcal{E}_{\mathrm{B}}(\alpha, 1 - 2). \qquad (C19)$$

Then Eq. (18) yields

$$\tilde{\chi}_0(\alpha) = - \sum_{\gamma} \tilde{G}(\alpha + \gamma) \tilde{G}(\gamma) \tilde{\Lambda}(\gamma, \alpha) \qquad (C20)$$

and Eq. (17) yields

$$\tilde{\chi}^{\mathrm{cov}}(\alpha) = \frac{\tilde{\chi}_0(\alpha)}{1 + \tilde{V}(\alpha) \tilde{\chi}_0(\alpha)}. \qquad (C21)$$

Up to now, the covariant *HGW* Eqs. (C15), (C20), and (C21) are obtained in Fourier space for the Hubbard model.

APPENDIX D: CORRELATORS IN MATSUBARA ACTION

The Matsubara action given in Eq. (22) is dependent on the number of time slices M and tends to the continuous time limit,

$$S[\psi, \psi^*] = \sum_{i, \sigma} \int_0^\beta d\tau \, \psi_{i, \sigma}^*(\tau) \partial_\tau \psi_{i, \sigma}(\tau)$$

$$+ \int_0^\beta d\tau \, \mathcal{H}[\psi_{i\sigma}^*(\tau), \psi_{i\sigma}(\tau)], \qquad (D1)$$

with a convergence speed $1/M$. For a short formulation, the spin and space coordinates are dropped below. One can define the M-dependent Green's function as

$$G_M(\tau_{l_1}, \tau_{l_2}) \equiv \frac{1}{Z_M} \int \mathcal{D}[\psi, \psi^*] \, \psi^*(\tau_{l_2}) \psi(\tau_{l_1}) e^{-S_M[\psi, \psi^*]},$$

$$(D2)$$

with the partition function

$$Z_M \equiv \int \mathcal{D}[\psi, \psi^*] \, e^{-S_M[\psi, \psi^*]}. \qquad (D3)$$

Since, as M tends to infinity, $S_M[\psi, \psi^*]$ tends to $S[\psi, \psi^*]$ with a convergence speed $\frac{1}{M}$, then $G_M(\tau_{l_1}, \tau_{l_2})$ tends to $G(l_1\beta/M, (l_2 + 1)\beta/M)$ with the same convergence speed. For this reason, one can approximate that in the continuous time limit,

$$G\left(\frac{l_1}{M}\beta, \frac{l_2 + 1}{M}\beta\right) = 2G_{2M}(\tau_{2l_1}, \tau_{2l_2+1}) - G_M(\tau_{l_1}, \tau_{l_2}).$$

$$(D4)$$

Define the M-dependent particle density as

$$\rho_M(\tau_l) \equiv G_M(\tau_l, \tau_l). \qquad (D5)$$

As M tends to infinity, it tends to the particle density in the continuous time limit. Then one can conclude that the M-dependent particle density ρ_M tends to the particle density ρ with a convergence speed $1/M$ as M tends to infinity. Therefore, one can approximate that

$$\rho(l\beta/M) = 2\rho_{2M}(\tau_{2l}) - \rho_M(\tau_l). \qquad (D6)$$

Equations (D4) and (D6) help to lower down the error of $O(1/M)$ caused by finite M to $O(1/M^2)$.

APPENDIX E: ALGORITHM

1. Routine for the Green's function

The *HGW* Eqs. (C9) are mathematically nonlinear equations of the Green's function $\tilde{G}$. To solve the nonlinear

equations, one can use the Broyden algorithm [44]. The Broyden algorithm is designed to solve the nonlinear equations $F[X] = 0$ with an initial value $X = X_0$. This algorithm mainly contains two inputs, the nonlinear function F, and the initial value X_0. In our cases, X stands for the Green's function $\tilde{G}$, and F stands for $\tilde{G}' - \tilde{G}$, where $\tilde{G}'$ is given by

$$\tilde{G}' = \frac{1}{\tilde{H}^{-1} + \mathcal{C}[\tilde{H}, \frac{1}{\tilde{V}^{-1} - \mathcal{C}[\tilde{H}, \tilde{G}]}]}, \tag{E1}$$

with the correlation functional

$$\mathcal{C}[\tilde{X}, \tilde{Y}](\alpha) \equiv \frac{1}{\mathcal{N}} \sum_\gamma \tilde{X}(\alpha + \gamma) \tilde{Y}(\gamma), \tag{E2}$$

and X_0 stands for the initial value given by

$$\tilde{G}_0(\alpha) = \frac{1}{T(\alpha) - \frac{U}{2}\rho_0 - \Sigma_0(\alpha)}, \tag{E3}$$

where the initial particle density $\rho_0 \in (0, 2)$ is given randomly, and the initial self-energy Σ_0 is also given randomly. Note that the correlation Eq. (E2) can be fastened by discrete Fourier transformation algorithm [44] and, as a result, the complexity of one iteration Eq. (E1) is $O(N \log N)$.

There might be multiple solutions to the nonlinear equations. In our calculations, only one solution is found in the case that U/t is sufficiently small or βt is sufficiently small. However, multiple solutions are found in the case of strong coupling and low temperature. Our strategy is setting gradients to U or β and then solving the Green's function with different initial values for each parameter, and finally choosing the solution continuous with U or β.

To eliminate the error of $1/M$ of the Green's function in Matsubara time, one can set different numbers of Matsubara time slices and then make extrapolation. In our calculations, M is set to 512, 1024, and 2048. To show M is sufficiently large, one can verify $(2\rho_{2048} - \rho_{1024}) - (2\rho_{1024} - \rho_{512})$ is close to zero. To obtain the density, one can use the approximation $\rho \doteq 2\rho_{2048} - \rho_{1024}$. To obtain the Green's function, one uses

$$G\left(\frac{l_1}{1024}\beta, \frac{l_2 + 1}{1024}\beta\right) = 2G_{2048}(\tau_{2l_1}, \tau_{2l_2+1}) - G_{1024}(\tau_{l_1}, \tau_{l_2}). \tag{E4}$$

Clearly, the Green's function on only discrete Matsubara time can be obtained. In addition, the particle density n per site relates to ρ through the relation

$$n \equiv n_i(\tau) = \rho_{i\uparrow}(\tau) + \rho_{i\downarrow}(\tau). \tag{E5}$$

The numerical cost of the calculation of the Green's function is analyzed as follows. For $U = 2, T = 0.125$ at half filling and $M = 1024, N = 16$, the typical numerical cost is about 2.3 s running on a 32-core CPU(2.6 GHz). The numerical cost is almost proportional to MN^2 and thus is applicable to complicated systems.

The parameters U and T influence the number of iterations, and then influence the numerical cost. We set $M = 1024$ and $N = 16$. The numerical costs dependent on U at $T = 0.125$ are presented in Table II and the results demonstrate that the numerical cost might be exponential in the Hubbard U. The numerical costs dependent on T at $U = 2$ are presented in Table III and the results demonstrate that the numerical

TABLE II. Dependence of the numerical cost on the Hubbard U.

U	2.0	2.5	3.0	3.5	4.0
Cost (seconds)	2.257	5.919	7.743	16.429	38.945

cost is almost linear in $1/T$. In addition, for good precision, one should increase M as U increases or T decreases. According to our experience, setting $M = \lceil 16 \times U/T \rceil$ yields a satisfactory precision [after the extrapolation Eq. (D4)]. With these factors in consideration, the *HGW* method should be applicable to the cases at sufficiently low temperature but not very large U.

2. Routine for the density-density correlator

In the routine for the density-density correlator, there are mainly three steps. First, calculate $\tilde{H}, \tilde{W}$ for given $\tilde{G}$ and parameters. Second, construct $\mathcal{M}$ and b, and solve the linear Eq. (C15) to obtain $\tilde{\Lambda}$. Third, calculate $\tilde{\chi}_0$ using Eq. (C20), and calculate $\tilde{\chi}^{\text{cov}}$ using Eq. (C21). The second step has the largest complexity, up to $O(N^4)$. The linear equations can be solved iteratively in a much faster speed than the linear system solver.

The charge correlator χ^{ch} relates to χ through the relation

$$\chi^{\text{ch}}_{i_1, i_2}(\tau_1, \tau_2) \equiv \langle n_{i_1}(\tau_1) n_{i_2}(\tau_2) \rangle - \langle n_{i_1}(\tau_1) \rangle \langle n_{i_2}(\tau_2) \rangle$$
$$= \sum_{\sigma_1, \sigma_2} \chi_{i_1\sigma_1, i_2\sigma_2}(\tau_1, \tau_2). \tag{E6}$$

Note that

$$\chi_{i_1\sigma_1, i_2\sigma_2}(\tau_1, \tau_2) = \langle \rho_{i_1\sigma_1}(\tau_1) \rho_{i_2\sigma_2}(\tau_2) \rangle - \langle \rho_{i_1\sigma_1}(\tau_1) \rangle \langle \rho_{i_2\sigma_2}(\tau_2) \rangle. \tag{E7}$$

The charge susceptibility $\chi_c \equiv \partial n / \partial \mu$ in discrete time Matsubata action should satisfy

$$\chi_c = \Delta\tau \sum_{l=0}^{M-1} \sum_i \langle nn_i(\tau_l) \rangle_c = \Delta\tau \tilde{\chi}^{\text{ch}}(0, 0), \tag{E8}$$

with the (discrete) Fourier transformation

$$\chi^{\text{ch}}_{i_1 i_2}(\tau_1, \tau_2) = \frac{1}{MN^2} \sum_{k,m} \tilde{\chi}^{\text{ch}}(k, m) e^{ik \cdot (i_1 - i_2)} e^{i\pi 2m \cdot (\tau_1 - \tau_2)}. \tag{E9}$$

The numerical cost of calculation of the two-body correlators is analyzed as follows. For $M = 1024, N = 4$, the typical numerical cost is about 3 h running on a 32-core CPU(2.6 GHz). The numerical cost is almost proportional to the square of MN^2, and is almost independent of U and T. The numerical cost is a bit large, and is not applicable to realistic materials with the current algorithm.

TABLE III. Dependence of the numerical cost on the inverse temperature.

$1/T$	8.0	16.0	24.0	32.0
Cost (seconds)	2.367	3.523	7.497	10.967

APPENDIX F: *GW* EQUATIONS

The *GW* approximation is based on Hedin's equations

$$G^{-1}(1, 2) = H^{-1}(1, 2) - \Sigma(1, 2),$$

$$\Sigma(1, 2) = -\int d(34)\, G(1, 4)W(3, 1)\Lambda(4, 2; 3),$$

$$W^{-1}(1, 2) = V^{-1}(1, 2) - \Pi(1, 2),$$

$$\Pi(1, 2) = \int d(34)\, G(1, 3)G(4, 1)\Lambda(3, 4; 2), \quad \text{(F1)}$$

with Hedin's vertex $\Lambda(1, 2; 3) = \delta G^{-1}(1, 2)/\delta v(3)$.

One can make the simplest approximation for Hedin's vertex Λ,

$$\Lambda(1, 2; 3) \doteq \delta H^{-1}(1, 2)/\delta v(3) = \delta(1, 2)\delta(1, 3),$$

to obtain the *GW* equations:

$$G^{-1}(1, 2) = H^{-1}(1, 2) - \Sigma(1, 2),$$

$$\Sigma(1, 2) = -G(1, 2)W(2, 1),$$

$$W^{-1}(1, 2) = V^{-1}(1, 2) - \Pi(1, 2),$$

$$\Pi(1, 2) = G(1, 2)G(2, 1). \quad \text{(F2)}$$

[1] M. Imada, A. Fujimori, and Y. Tokura, Metal-insulator transitions, Rev. Mod. Phys. **70**, 1039 (1998).

[2] A. Auerbach, *Interacting Electrons and Quantum Magnetism* (Springer Science & Business Media, New York, 2012).

[3] T. Timusk and B. Statt, The pseudogap in high-temperature superconductors: An experimental survey, Rep. Prog. Phys. **62**, 61 (1999).

[4] P. A. Lee, N. Nagaosa, and X. G. Wen, Doping a Mott insulator: Physics of high-temperature superconductivity, Rev. Mod. Phys. **78**, 17 (2006).

[5] E. Dagotto, Correlated electrons in high-temperature superconductors, Rev. Mod. Phys. **66**, 763 (1994).

[6] D. J. Scalapino, A common thread: The pairing interaction for unconventional superconductors, Rev. Mod. Phys. **84**, 1383 (2012).

[7] J. Hubbard, Electron correlations in narrow energy bands, Proc. R. Soc. London Ser. A, Math. Phys. Sci. **276**, 238 (1963).

[8] U. Schollwock, The density-matrix renormalization group, Rev. Mod. Phys. **77**, 259 (2005).

[9] F. Becca and S. Sorella, *Quantum Monte Carlo Approaches for Correlated Systems* (Cambridge University Press, Cambridge, 2017).

[10] A. Georges, G. Kotliar, W. Krauth, and M. J. Rozenberg, Dynamical mean-field theory of strongly correlated fermion systems and the limit of infinite dimensions, Rev. Mod. Phys. **68**, 13 (1996).

[11] G. Kotliar, S. Y. Savrasov, K. Haule, V. S. Oudovenko, O. Parcollet, and C. A. Marianetti, Electronic structure calculations with dynamical mean-field theory, Rev. Mod. Phys. **78**, 865 (2006).

[12] G. Rohringer, H. Hafermann, A. Toschi, A. A. Katanin, A. E. Antipov, M. I. Katsnelson, A. I. Lichtenstein, A. N. Rubtsov, and K. Held, Diagrammatic routes to nonlocal correlations beyond dynamical mean field theory, Rev. Mod. Phys. **90**, 025003 (2018).

[13] T. Schäfer, N. Wentzell, F. Simkovic, Y.-Y. He, C. Hille, M. Klett, C. J. Eckhardt, B. Arzhang, V. Harkov, F.-M. Le Regent, A. Kirsch, Y. Wang, A. J. Kim, E. Kozik, E. A. Stepanov, A. Kauch, S. Andergassen, P. Hansmann, D. Rohe, Y. M. Vilk *et al.*, Tracking the Footprints of Spin Fluctuations: A MultiMethod, MultiMessenger Study of the Two-Dimensional Hubbard Model, Phys. Rev. X **11**, 011058 (2021).

[14] G. Baym and L. Kadanoff, Conservation laws and correlation functions, Phys. Rev. **124**, 287 (1961).

[15] G. Baym, Self-consistent approximations in many-body systems, Phys. Rev. **127**, 1391 (1962).

[16] L. Hedin, New method for calculating the one-particle Green's function with application to the electron-gas problem, Phys. Rev. **139**, A796 (1965).

[17] C. Dedominicis and P. Martin, Stationary entropy principle and renormalization in normal and superfluid systems. 2. Diagrammatic formulation, J. Math. Phys. **5**, 31 (1964).

[18] L. Kadanoff and P. Martin, Theory of many-particle systems. 2. Superconductivity, Phys. Rev. **124**, 670 (1961).

[19] Q. J. Chen, J. Stajic, S. Tan, and K. Levin, BCS-BEC crossover: From high temperature superconductors to ultracold superfluids, Phys. Rep. **412**, 1 (2005).

[20] B. Rosenstein and D. Li, Covariant cubic approximation for many-body electronic systems, Phys. Rev. B **98**, 155126 (2018).

[21] F. Aryasetiawan and O. Gunnarsson, The GW method, Rep. Prog. Phys. **61**, 237 (1998).

[22] N. E. Bickers, D. J. Scalapino, and S. R. White, Conserving Approximations for Strongly Correlated Electron Systems: Bethe-Salpeter Equation and Dynamics for the Two-Dimensional Hubbard Model, Phys. Rev. Lett. **62**, 961 (1989).

[23] C. Dedominicis and P. Martin, Stationary entropy principle and renormalization in normal+superfluid Systems. I. Algebraic formulation, J. Math. Phys. **5**, 14 (1964).

[24] N. E. Bickers and S. R. White, Conserving approximations for strongly fluctuating electron systems. II. Numerical results and parquet extension, Phys. Rev. B **43**, 8044 (1991).

[25] Z. Fan, Z. Sun, D. Li, I. Berenstein, G. Leshem, and B. Rosenstein, Covariant Bethe-Salpeter approximation in models of strongly correlated electron systems, Phys. Rev. E **101**, 023310 (2020).

[26] A. L. Kutepov and G. Kotliar, One-electron spectra and susceptibilities of the three-dimensional electron gas from self-consistent solutions of Hedin's equations, Phys. Rev. B **96**, 035108 (2017).

[27] K. Morita, H. Maebashi, and K. Miyake, FLEX study on the compressibility of the two-dimensional Hubbard model, Phys. B: Condens. Matter **312**, 547 (2002).

[28] A. Kovner and B. Rosenstein, Covariant Gaussian approximation.1. Formalism, Phys. Rev. D **39**, 2332 (1989).

[29] B. Rosenstein and A. Kovner, Covariant Gaussian approximation. 2. Scalar theories, Phys. Rev. D **40**, 504 (1989).

[30] J. F. Wang, D. P. Li, H. C. Kao, and B. Rosenstein, Covariant gaussian approximation in Ginzburg-Landau model, Ann. Phys. **380**, 228 (2017).

[31] J. W. Negele, *Quantum Many-Particle Systems* (CRC Press, Boca Raton, Florida, USA, 2018).

[32] J. Fei, C.-N. Yeh, and E. Gull, Nevanlinna Analytical Continuation, Phys. Rev. Lett. **126**, 056402 (2021).

[33] N. Bulut, D. J. Scalapino, and S. R. White, One-Electron Spectral Weight of the Doped Two-Dimensional Hubbard Model, Phys. Rev. Lett. **72**, 705 (1994).

[34] A. Tanaka, Metal-insulator transition in the two-dimensional Hubbard model: Dual fermion approach with Lanczos exact diagonalization, Phys. Rev. B **99**, 205133 (2019).

[35] B. Kyung, G. Kotliar, and A. M. S. Tremblay, Quantum Monte Carlo study of strongly correlated electrons: Cellular dynamical mean-field theory, Phys. Rev. B **73**, 205106 (2006).

[36] D. Sénéchal, D. Perez, and M. Pioro-Ladrière, Spectral Weight of the Hubbard Model through Cluster Perturbation Theory, Phys. Rev. Lett. **84**, 522 (2000).

[37] T. Ayral and O. Parcollet, Mott physics and spin fluctuations: A unified framework, Phys. Rev. B **92**, 115109 (2015).

[38] T. Ayral and O. Parcollet, Mott physics and spin fluctuations: A functional viewpoint, Phys. Rev. B **93**, 235124 (2016).

[39] J. Vucicevic, T. Ayral, and O. Parcollet, TRILEX and GW plus EDMFT approach to d-wave superconductivity in the Hubbard model, Phys. Rev. B **96**, 104504 (2017).

[40] Y. M. Vilk and A.-M. S. Tremblay, Non-perturbative many-body approach to the Hubbard model and single-particle pseudogap, J. Phys. I France **7**, 1309 (1997).

[41] H. Miyahara, R. Arita, and H. Ikeda, Development of a two-particle self-consistent method for multiorbital systems and its application to unconventional superconductors, Phys. Rev. B **87**, 045113 (2013).

[42] K. Zantout, S. Backes, and R. Valentí, Two-particle self-consistent method for the multi-orbital Hubbard model, Ann. Phys. **533**, 2000399 (2021).

[43] M. Peskin, *An Introduction to Quantum Field Theory* (CRC Press, Boca Raton, Florida, USA, 2018).

[44] W. H. Press, S. A. Teukolsky, W. T. Vetterling, and B. P. Flannery, *Numerical Recipes: The Art of Scientific Computing*, 3rd ed. (Cambridge University Press, Cambridge, 2007).